

NJC

Accepted Manuscript



This is an *Accepted Manuscript*, which has been through the Royal Society of Chemistry peer review process and has been accepted for publication.

Accepted Manuscripts are published online shortly after acceptance, before technical editing, formatting and proof reading. Using this free service, authors can make their results available to the community, in citable form, before we publish the edited article. We will replace this *Accepted Manuscript* with the edited and formatted *Advance Article* as soon as it is available.

You can find more information about *Accepted Manuscripts* in the [Information for Authors](#).

Please note that technical editing may introduce minor changes to the text and/or graphics, which may alter content. The journal's standard [Terms & Conditions](#) and the [Ethical guidelines](#) still apply. In no event shall the Royal Society of Chemistry be held responsible for any errors or omissions in this *Accepted Manuscript* or any consequences arising from the use of any information it contains.



www.rsc.org/njc

Plasmonic Coinage Metal-TiO₂ Hybrid Nanocatalysts for Highly Efficient Photocatalytic Oxidation under Sunlight Irradiation

Author's name: Rupinder Kaur and Bonamali Pal*

The affiliation and address of the authors:

Dr. Bonamali Pal
Professor and Head
School of Chemistry and Biochemistry
Thapar University
Patiala 147004
Punjab
INDIA

Dr. Rupinder Kaur
Women Scientist-A
Thapar University
Patiala 147004
Punjab
INDIA

Corresponding author:
Dr. Bonamali Pal
E-mail: bpal@thapar.edu
Tel: + 91-175-2393491
Fax: + 91-175-2364498

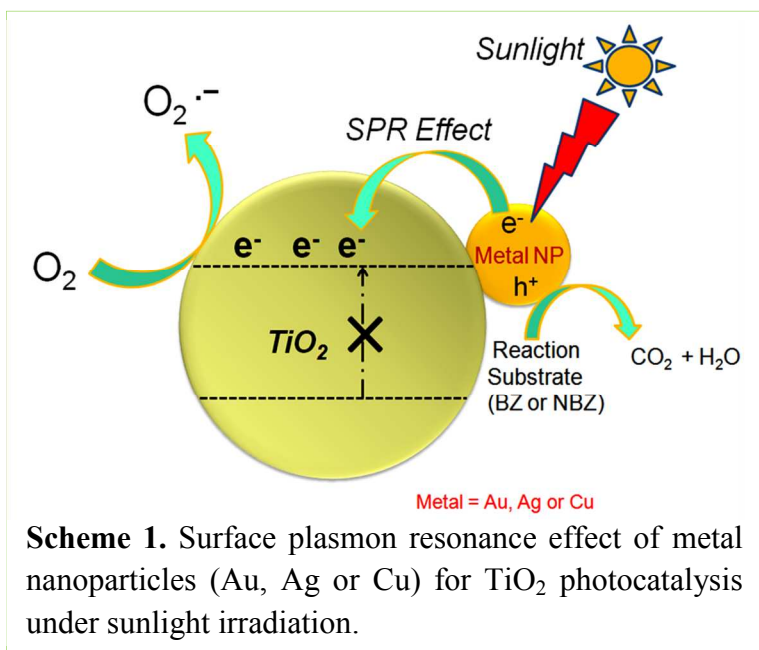
Abstract:

The conventional methods of Au co-catalyst deposition onto TiO₂ surface generally does not offer fine tuning of metal-TiO₂ interface for enhanced photoactivity because of non-uniform distribution of different size and shape of metal nanodeposits. Hence, this study demonstrated the comparative co-catalysis activity imparted to TiO₂ by as prepared coinage metal (Au, Ag and Cu) quantum dot particles of similar sizes (3-5 nm) as a function of their plasmonic interactions with TiO₂ under visible light irradiation. The physiochemical and interfacial properties of metal-TiO₂ composites are studied by optical band gap, XRD, XPS, TEM, surface area, time resolved spectroscopy, current-voltage characteristics, GC and GC-MS analysis. It revealed that optical band gap is shifted to 2.9 eV from 3.2 eV of bare TiO₂ and the specific surface area 50 m²g⁻¹ of TiO₂ is notably reduced to 20-33 m²g⁻¹ after metal nanoparticles impregnation (M-TiO₂) that found to exist as Au⁰ and Ag⁰, and Cu⁺² oxidation state. The average relaxation time \approx 18 μ s (bare TiO₂) < 20 μ s (Cu-TiO₂) < 24 μ s (Au-TiO₂) < 27 μ s (Ag-TiO₂) of photoexcited charge species and the highest conductance value 1.65×10^{-7} S of Ag-TiO₂ as revealed by current-voltage studies strongly established that Ag-TiO₂ interface acts as a better electron sink to capture and store photogenerated electrons, thus displaying superior photocatalytic activity than Au/or Cu-TiO₂ interface. Thus Ag-TiO₂ exhibited the highest rate constant $k = 4 \times 10^{-2} \text{ min}^{-1}$ relative to $k = 2.7 \times 10^{-2} \text{ min}^{-1}$ (Au-TiO₂) and $k = 1.93 \times 10^{-2} \text{ min}^{-1}$ (Cu-TiO₂) for the oxidative degradation of benzaldehyde and nitrobenzadhyde to CO₂ under direct sunlight (40-50 mW/cm²) exposure.

Keywords: Metal-TiO₂ interfacial energetics; Coinage metal-TiO₂ nanocomposites; Plasmonic nanoparticles; Plasmonic interaction; Visible light photoactivity.

1. Introduction

TiO₂ (band gap = 3.2 eV) has been known as a most promising photocatalyst material¹⁻³ utilized in many practical applications despite its limitation of light absorption capacity ($\lambda = 388$ nm) in the UV range. Hence, different techniques viz; metal and non-metal doping^{4,5}, photo-deposition⁶⁻⁸, dye



sensitization⁹ or coupling with different semiconductor materials¹⁰⁻¹² have been adopted to enhance the light absorption sensitivity and improve the photoactivity under solar irradiation for many viable uses. In this respect, coinage metals (Au, Ag, and Cu etc.) deposition onto TiO₂ is recently being investigated because of their characteristic surface plasmon resonance band (SPR)¹³⁻²⁴ absorbing light in the visible region, which stimulate an efficient transfer of the photo-excited electrons from metal particles to the conduction band of TiO₂. This would result in electron-deficiency in metal and electron-richness in TiO₂ and therefore, the photocatalytic oxidation occurs on the metal surface rather than on TiO₂ surfaces as shown in scheme 1.

The use of Au-TiO₂ photocatalysts for visible-light hydrogen generation due to their strong plasmonic near-fields localization close to the Au-TiO₂ interface has been demonstrated by Seh et al.²⁵ Zheng et al.⁹ prepared noble-metal plasmonic photocatalysts M@TiO₂ (M=Au, Pt, Ag) for carrying out the photocatalytic reactions under visible-light. Pd nanoparticles (NPs) were synthesized directly on commercial TiO₂ by gamma radiolysis to study their influence on the

formation and decay of charge-carriers and photoactivity of photocatalyst has been studied for the degradation of phenol and rhodamine B under UV and visible light²⁶. The Ag/AgCl/TiO₂ nanotube arrays²⁷ have been prepared by depositing AgCl NPs into the self-organized TiO₂ nanotubes for photodegradation of methyl orange. Hybrid photocatalysts composed of plasmonic NPs, titania and ruthenium have been prepared for decomposition of organic compounds, chemical and biological pollutants, etc. under solar radiation^{28,29}. Grabowska et al.³⁰ modified titanium(IV)dioxide with silver NPs to obtain efficient photocatalysts with higher photoactivity under solar irradiation. P25-TiO₂ modified with bimetallic Au-Cu nanoparticles prepared by employing deposition–precipitation followed by radiolytic reduction has been utilized for photodegradation of phenol³¹ under UV and visible light illumination. Stable one-dimensional poly(diphenylbutadiyne) nanostructures have been synthesized by photopolymerization using a soft templating approach showed high photocatalytic activity under visible light without the assistance of sacrificial reagents³². Tsukamoto et al.³³ observed efficient aerobic oxidation of 1-phenylethanol at room temperature using Au nanoparticles loaded to a mixture of anatase/rutile TiO₂ particles (Degussa, P25) under visible-light irradiation ($\lambda > 450$ nm).

It was found that most of these conventional approaches failed to present the uniform distribution of quantum size metal particles on the TiO₂ surface for the fine tuning of metal-TiO₂ interface and enhanced photoactivity. Therefore, it is desirable to prepare coinage metal NPs separately and introducing them on TiO₂ matrix which offers beneficial advantages over typical metal loading techniques that generally led to the deposition of aggregated metal nanodeposits over TiO₂ particles. As every metal NP has its unique property such as Ag and Au exhibit capacitive properties, whereas Pt and Pd provide an ohmic contact³⁴ to the SC. Silver is known as the most important material in plasmonics as it offers strong SPR³⁵ at the desired resonance

wavelength across the spectrum (300 to 1200 nm). Therefore, it is desirable to know that how the nature of coinage metal NPs influences the interfacial energetics and photoefficiency of metal-TiO₂ composites as a function of their size and shape dependent plasmon resonance band.

In this context, Au, Ag and Cu nanospheres of similar sizes ($\approx 3-5$ nm) have been prepared and impregnated separately on TiO₂ to study their charge transfer processes at the metal-TiO₂ interface (Scheme 1), electron storage capacity, work function, Fermi-level shift, oxidation state and the nature of the coinage metal NPs. Various techniques such as optical (UV-vis spectra), structural (TEM, EDX, XRD, surface area), XPS, time resolved spectroscopy, and current-voltage characteristics have been widely studied to obtain various physicochemical properties of different coinage metal nanoparticles-TiO₂ binary composites. Their comparative photocatalytic activity is studied for the oxidative degradation of toxic and carcinogenic compounds such as benzaldehyde and nitrobenzaldehyde to various intermediate products and their complete mineralization to CO₂ under direct sunlight irradiation.

2. Experimental section

2.1 Materials and methods

Chloroauric acid, copper sulphate, trisodium citrate, benzaldehyde (BZ), nitrobenzaldehyde (NBZ) was purchased from Loba chemicals. Silver nitrate (AgNO₃) was purchased from Fischer scientific and commercially available P25-TiO₂ was obtained from Degussa Corporation, Germany, respectively. Deionized water with a measured conductivity 35 mho cm⁻¹ at 25°C was obtained by using an ultra filtration system (Milli-Q, Millipore).

2.2 Synthesis of Au, Ag and Cu nanospheres

Nanospheres (NS) of coinage metals (Au, Ag and Cu) have been prepared through chemical reduction route using trisodium citrate as a reducing as well as capping agent³⁶. The synthesis

procedure involves the addition of 140 μl (0.01 M) aqueous solution of HAuCl_4 , AgNO_3 , and CuSO_4 in three respective beakers containing 14 ml boiling solution of trisodium citrate (50 mg/ml). The obtained solution was allowed to boil till the light pink, yellow and brown color appears for the Au, Ag and Cu nanospheres, respectively.

2.3 Synthesis of M-TiO₂ nanocomposites (M = Au, Ag and Cu)

Metal impregnated titania nanocomposites (NC) were synthesized through wet impregnation method. 500 mg TiO_2 was mixed with 50 ml distilled water by adding requisite amounts (1 wt%) of metal nanospheres (Au, Ag and Cu) separately in three beakers, stirred overnight and then followed by drying at 100 °C. The dried powder catalyst was then repeatedly washed with water and all the prepared samples were sintered in a muffle furnace at 80°C for 10 h. The M-TiO₂ NC displayed a variety of colors depending on the nature of metal NPs present.

2.4 Photocatalytic activity

The photocatalytic activity was tested for the photooxidation of 10 ml benzaldehyde (BZ, 0.1 mM) and nitrobenzaldehyde (NBZ, 0.1 mM) with 20 mg catalysts (bare TiO_2 , Au-TiO₂, Ag-TiO₂ and Cu-TiO₂) under sunlight (intensity \approx 40-50 mW/cm^2) irradiation with constant magnetic stirring. The sunlight intensity (flux) was measured directly by placing Lux meter (LX-101) under the sunlight exposure on the terrace between 12.00 pm-3.00 pm. The reaction samples were analyzed by UV-vis spectrophotometer (λ_{max} = 260 nm for NBZ and 242 nm for BZ) after filtration with 0.22 μm cellulose filter. Intermediates formed during the photodegradation process were analyzed through GC-MS. The amount of CO_2 produced on mineralization of BZ and NBZ was measured by GC with TCD as a detector.

2.5 Characterization

The as prepared aqueous colloidal solution of metal NS (Au, Ag and Cu) and powdered M-TiO₂ composites were characterized by UV-vis absorption spectrophotometry (Analytikjena Specord 205) and diffuse reflectance spectrophotometer (Avantes Diffuse Reflectance Spectrophotometer), respectively. Morphological study of size analysis was done by dynamic light scattering (DLS, Brookhaven 90 plus instrument) and TEM. BET surface area was measured (Smartsorb 92/93 instrument) by N₂ adsorption technique. X-ray diffraction study (PANalytica X'pert PRO X-ray diffractometer) was carried out for phase identifications. XPS (PHI 5200 mode) was done for surface elemental studies. Current voltage characteristics (KI 2400) and Time resolved spectroscopy (Tektronix TDS-1012 oscilloscope) were also investigated.

3. Results and discussion

3.1 Optical and structural characteristics of metal nanospheres

Figure 1 displayed the surface plasmon resonance (SPR) bands for Au (≈ 520 nm), Ag (≈ 425 nm) and CuNS (~ 612 nm), respectively. Highly intense and sharp band has been observed for Au and AgNS, whereas weak and broadened band was depicted for CuNS. Such SPR band for AgNS at 420 nm has also been observed by Ratyakshi et al.³⁷, employing trisodium citrate as a reducing agent, showing the size range ≈ 10 -20 nm. AuNS of size ≈ 3 -5 nm (SPR band ≈ 520 nm) has been prepared by well

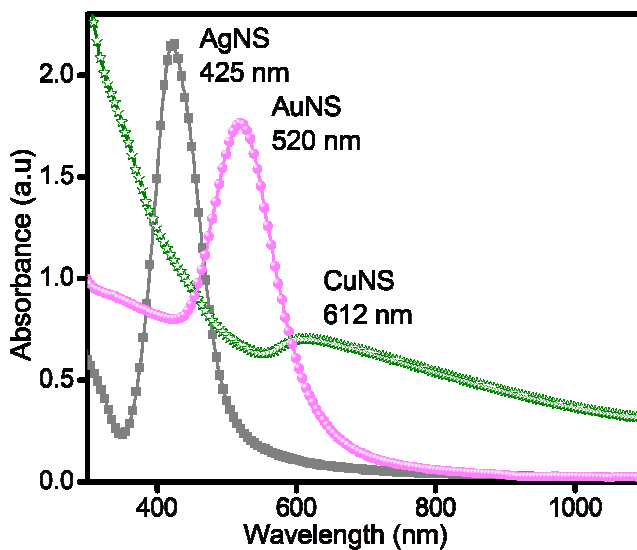


Figure 1. Surface plasmon resonance band for Au, Ag and Cu nanospheres.

known Turkevich method³⁸, using citrate as a reducing and capping agent. Samim et al.³⁹ reported the preparation of CuNS of various sizes by citrate reduction route. The sharp band for Au and AgNS suggests the presence of homogenous and well separated particles while broadening in the SPR band for CuNS signifies its larger size.

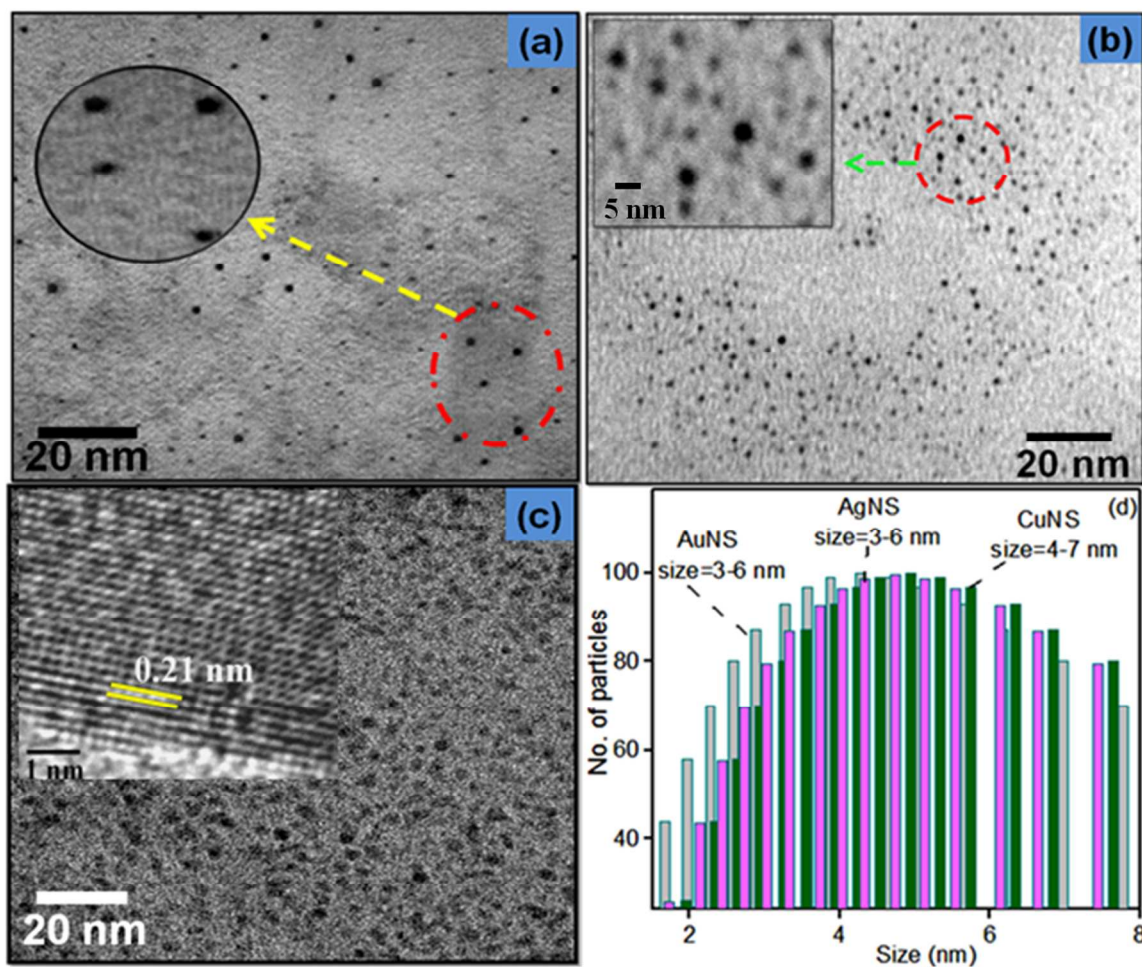


Figure 2. TEM images of (a) Au, (b) Ag, (c) Cu nanospheres and (d) their DLS particle size distribution plot.

TEM micrographs of AuNS (Fig. 2a) revealed that all the particles are spherical in shape, well dispersed having average size \approx 3-5 nm. The inset Fig. 2a showed the magnified image of AuNS which insure their rounded/spherical shape. The homogeneously dispersed NS of Ag are lying well separated from each other and displaying size range \approx 3-5 nm (Fig. 2b). CuNS of similar

size \approx 3-5 nm with spherical morphology has been shown in Fig. 2c. The high resolution transmission electron microscopic image (Inset fig. 2c) of as-synthesized copper nanoparticles showed d-spacing of lattice fringes is \approx 0.21 nm, which is in agreement with the value of (111) plane of fcc Cu as reported by Cheirmadurai et al⁴⁰. The DLS particle size distribution studies for all the prepared coinage metal (Au, Ag and Cu) NS has also been found to be in the range of 3-7 nm size as displayed in Fig. 2d. The histograms show the average particle sizes to be around 3.7, 4 and 4.3 nm respectively for Au, Ag and Cu nanoparticles as shown in electronic supplementary information (ESI)-Fig.S1.

3.2 Diffuse reflectance studies of M-TiO₂ composites

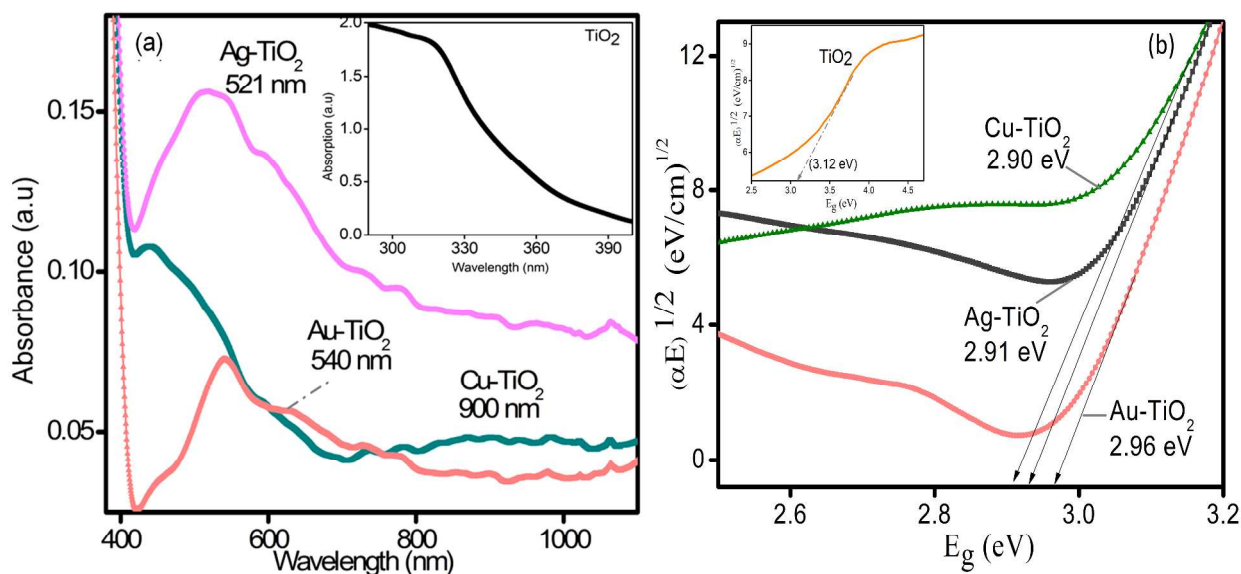


Figure 3. (a) Solid state absorbance spectra of bare TiO₂ (inset) and 1 wt% metal NP loaded M-TiO₂ (M = Au, Ag and Cu) composites and, (b) their respective bandgaps.

The UV-vis diffuse reflectance spectrum of M-TiO₂ NC relative to bare TiO₂ has been represented in Fig. 3a. TiO₂ NPs are characterized by absorption edge around \sim 390 nm (band gap, $E_g \approx$ 3.12 eV, inset Fig. 3a) and an alteration (\approx 390 to 415-420 nm) in the absorption edge of TiO₂ has been observed^{1-10,14,17,19,41} on the loading of coinage metal NS. The characteristic

SPR bands (Fig. 1) of Au, Ag and Cu NS at 425, 520 and 612 nm are also red shifted to ~ 521, 540 and 800 nm in their respective composite form^{20,42,43} (Au-TiO₂, Ag -TiO₂ and Cu-TiO₂). Red shift in the absorption edge of M-TiO₂ composites relative to bare TiO₂ is an indication of narrowing of the TiO₂ band gap. The band gap (E_g) of the M-TiO₂ has been determined from the Tauc plot by extrapolating the linear portion of the plot of $(\alpha h\nu)^2$ versus $h\nu$, showed in Fig. 3b. The E_g aids in determining the energy necessary to create electron-hole (e^-h^+) pairs in the semiconductor to initiate photocatalytic processes. E_g calculated using Tauc's equation was found to be ca. 2.96 eV, 2.91 eV and 2.90 eV for Au-TiO₂, Ag-TiO₂ and Cu-TiO₂, respectively (Table 1). It has been reported^{44,45} that the observed absorption edge shifting and band gap reduction in M-TiO₂ can be controlled as a function of surface morphology or by introducing lattice strain and vacancies.

3.3 TEM analysis of M-TiO₂ nanocomposites

The distribution of metal NS in M-TiO₂ NC and the way of their attachment to TiO₂ has been examined through TEM. Many black colored, spherical shaped AuNS in the size range 3-8 nm are seen to be uniformly distributed over TiO₂ (gray color) as shown in Fig. 4a-b. Similarly, AgNS and CuNS have been found to be scattered over the TiO₂ surface as shown in Fig. 4c-d and 4e, respectively. The size of the NS (Au and Ag) is found to be in good agreement with the average diameter of original colloidal solution before impregnating to TiO₂, verifying their non-aggregation behavior. One can observe from the images (Fig. 4a-e) that metal nanospheres are lying in a close proximity to TiO₂ and forming M-TiO₂ interfaces. Although there is no chemical bond between metal NS and TiO₂, probably the electrostatic attractions⁴⁶ between them bring them closer. The close contact formed at the interface of NPs and TiO₂ would facilitate the electron transfer in this composite photocatalyst and assist in the photoreaction systems. Metal-

support interactions^{47,48} might be the mode of interfacial contact between nanoparticles and TiO₂ as it has been reported⁴⁷ that electronic properties of the metals get modified while loading/impregnating on TiO₂ which was attributed to the overlapping of d-orbitals (occupied)

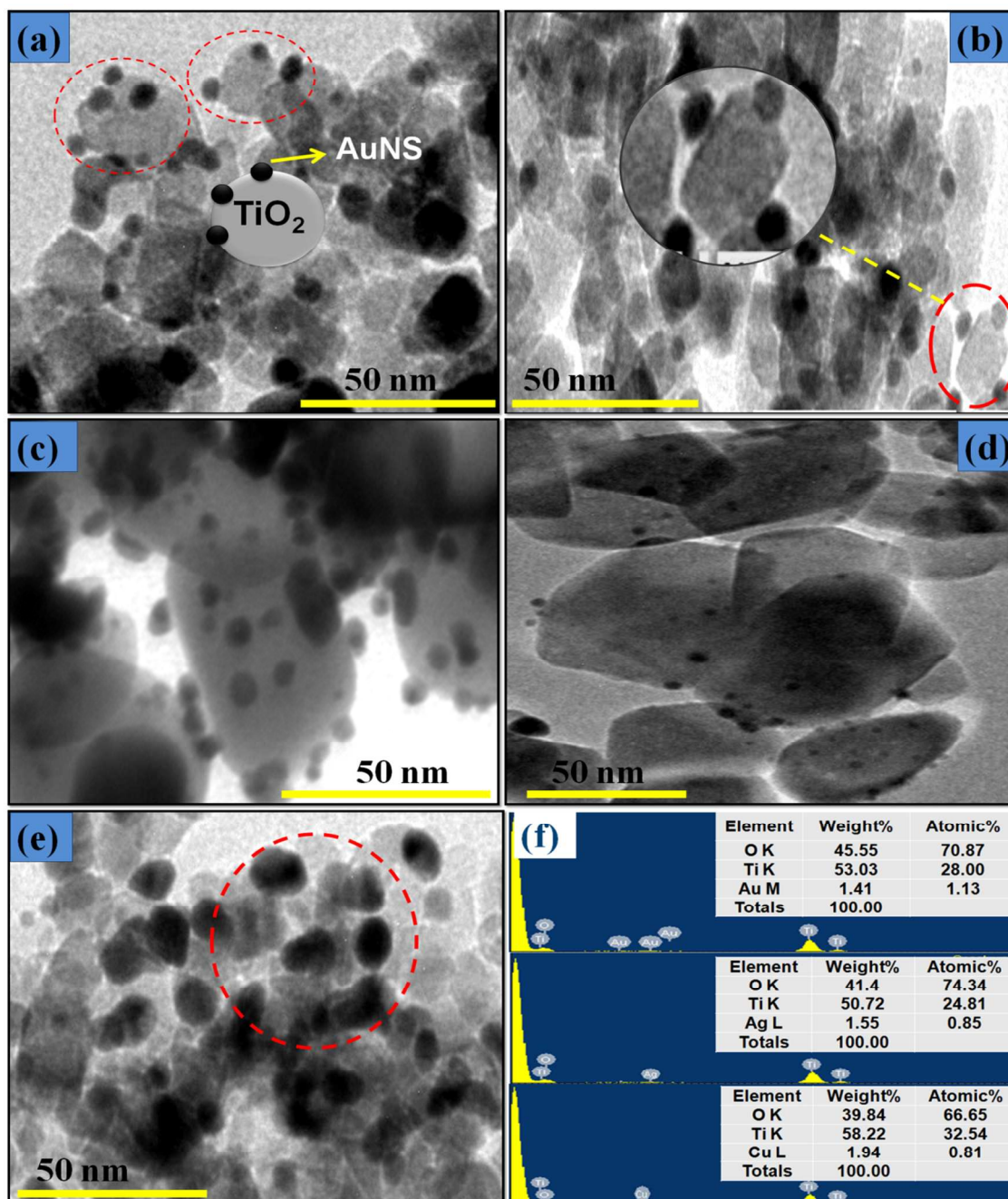


Figure 4. TEM images of 1 wt % (a,b) Au-TiO₂, (c,d) Ag-TiO₂, (e) Cu-TiO₂ composites and, (f) their respective EDX profiles.

from loaded metal and the unoccupied d-orbitals of the support. The elemental analysis carried out using EDX (Fig. 4f) confirms the presence of 1.13, 0.85 and 0.81 atomic % of Au, Ag and Cu in 1 wt % impregnated M-TiO₂ samples

3.4 XRD and BET analysis

The XRD analysis (ESI-Fig.S2) of M-TiO₂ NC in comparison to bare TiO₂ (P25) particles represents a mixture of anatase and rutile phase whereas, there is no any peak corresponding to metal NS has been observed. The non-existence of XRD peak for metal NS may be due to their lesser amount (≈ 1 wt%) and very small size (3-5 nm) which is below the detection limit. Moreover, the EDX and XPS analysis of the M-TiO₂ NC (ESI-Table 1) confirmed the presence of metal NPs. Similar observation has been reported by Zheng et al.⁹ on loading 1 wt% Au, Pt, Ag on TiO₂. However, XRD pattern of bare Au and Ag nanoparticle has been given in ESI-Fig.S3 that has been collected by freeze drying the nanoparticle solution. The presence of peaks at 2θ values 38.2°, 44.1°, 64.6° and 78.1° corresponds to (111), (200), (220) and (311) planes of Au (ESI-Fig.S3a), confirms its cubic structure⁴⁹, respectively. The diffraction patterns for Ag (ESI-Fig.S3b) revealed the diffraction peaks for cubic silver⁵⁰ at $2\theta = 38.1^\circ, 44.2^\circ, 64.4^\circ$ and 77.1° related to (111), (200), (220) and (311) planes, respectively.

Reduction in BET surface area ($S_{\text{BET}} = 29 \text{ m}^2\text{g}^{-1}$ for Au-TiO₂, $33 \text{ m}^2\text{g}^{-1}$ for Ag-TiO₂, and $20 \text{ m}^2\text{g}^{-1}$ for Cu-TiO₂ hybrid composites have been observed relative to $S_{\text{BET}} = 50 \text{ m}^2\text{g}^{-1}$ of bare TiO₂ which might be due to the partial surface coverage of titania porous sites with smaller metal NPs. Such results for the decrease in S_{BET} after deposition of metal particles over titania nanostructures were in agreement with the reported⁵¹ results.

3.5 XPS characterization

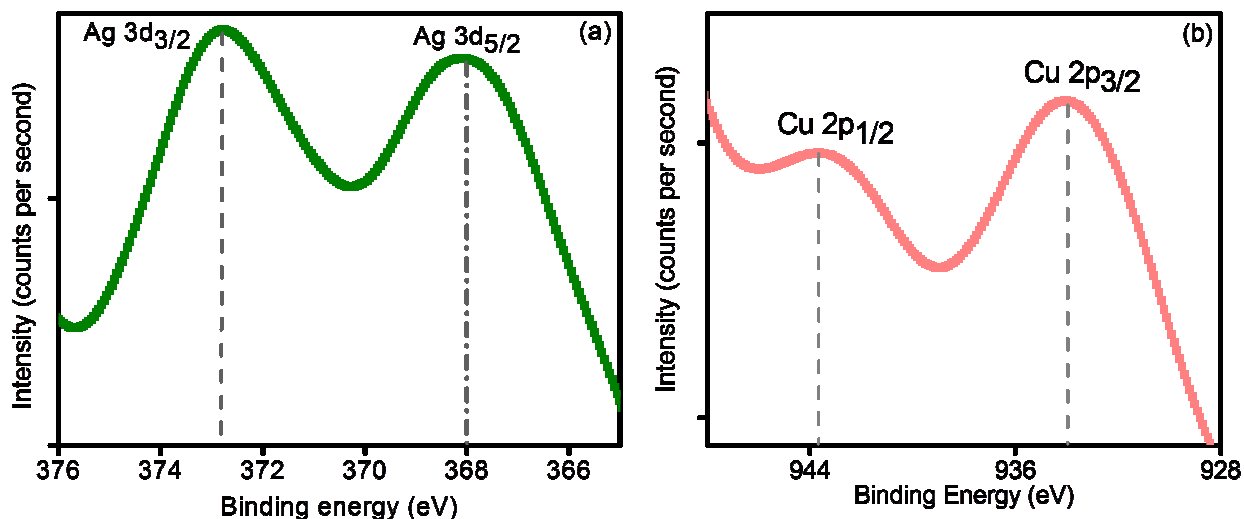


Figure 5. X-ray photoelectron spectra (XPS) of (a) Ag3d region for Ag-TiO₂ and (b) Cu2p region for Cu-TiO₂ nanocomposites.

The presence of coinage metal NPs, their respective surface chemical composition (atomic %) and oxidation state in M-TiO₂ NC was determined by XPS analysis^{23,52} as given in ESI-table 1. It has been observed that Ag-TiO₂ and Au-TiO₂ samples maintained O/Ti atom ratio very close to 3.5, indicating no variation in the metal oxide composition. However, for Cu-TiO₂, the O/Ti atom ratio is found close to ≈ 6 depicting the presence of some impurities in NC. The elemental composition has also shown C1s which may due to the adventitious hydrocarbon from the XPS instrument⁵³ itself. The full range XPS spectrum of Ag-TiO₂ contains three major peaks for O1s, Ti2p and Ag3d states (ESI-Fig.S4a). The XPS spectra of Ti (ESI-Fig.4b) shows two peaks located at 463.8 eV corresponds to Ti2p_{1/2} and the other one located at 458.1 eV has been assigned to Ti2p_{3/2}. The splitting between Ti2p_{1/2} and Ti-2p_{3/2} is around 5.6 eV, which is an indication of Ti⁴⁺ in the anatase phase of the Ag-TiO₂ NC⁵⁴. The O1s spectrum has two peaks located at 530 eV corresponds to the lattice oxygen of the Ag-TiO₂ and second peak at 531.6 eV (ESI-Fig.S4c), can be correlated to physisorbed water or -OH groups on the surface in [-

Ti(OH)-O-Ti-(OH)-] component⁵⁴. Deconvolution of Ag3d peaks (Fig. 5a) gives two bands at 373.6 eV and 368 eV that can be ascribed to Ag3d_{3/2} and Ag3d_{5/2} of the metallic silver^{23,55}, respectively. The binding energies of Au4f_{7/2} at 83.4 and Au4f_{5/2} at 87.7 eV are significantly different from Au⁺4f_{7/2} (84.6 eV) and Au³⁺4f_{7/2} (87.0 eV) which has been represented in ESI-Fig.S5, respectively. The result suggests that the Au species in Au-TiO₂ are in the metallic state as well stated in the reported^{23,56,57} results. The XPS spectrum for Cu2p (Fig. 5b) gives the binding energy of Cu2p at 933 eV and 943.4 eV corresponds to Cu2p_{3/2} and Cu2p_{1/2} which is characteristic of Cu²⁺ state⁵⁸ and its full range XPS spectrum can be seen in the ESI-Fig4d.

3.6 Current–voltage characteristics

The current–voltage (I–V) characteristics of the bare TiO₂ and M-TiO₂ heterojunctions are shown in Fig. 6a which found to follow the Ohm's law ($V=IR$). The observed data shows that with increasing voltage, flow of the current through the heterojunctions is also increasing and, therefore, corresponding I–V curve approaches a straight line with a slope equal to the resistance of the M-TiO₂ interface.

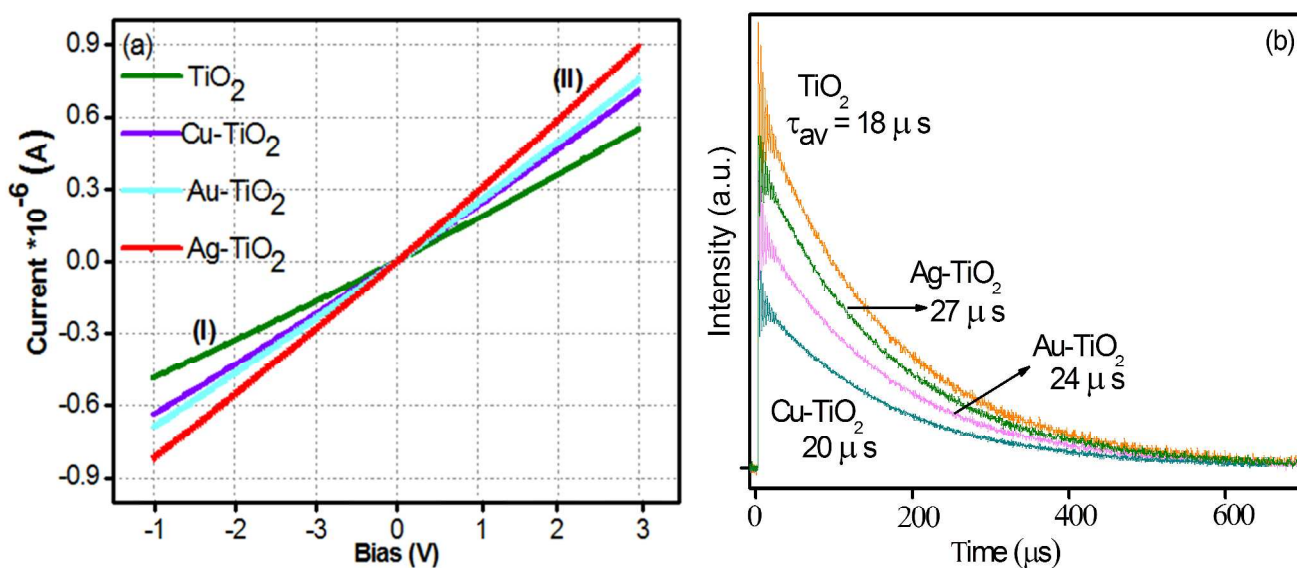


Figure 6. (a) Current-voltage (I–V curve) characteristic of bare TiO₂ and M-TiO₂ hetero-junctions and, (b) time resolved luminescence decay of bare TiO₂ and different M-TiO₂ composites.

This resistance was determined using the differential voltage method at large bias, I–V curve as $R = dV/dI$, where R is resistance, dV/dI differential voltage, this procedure gives resistances as 6.06, 3.70, 4.44 and 4.76 MΩ (at voltage = -2.0 V) and corresponding conductance values 1.65×10^{-7} , 2.7×10^{-7} , 2.25×10^{-7} and 2.1×10^{-7} S for bare, Ag-TiO₂, Au-TiO₂ and Cu-TiO₂ composites, respectively. This I–V curve can be divided into two or more segments, i.e., I and II, and, respective to these segments, the voltage (V), current (I), resistance (R) and conductance (S) has been calculated (Fig. 6a, ESI-table 2). The increase in conductance in M-TiO₂ composites in comparison to bare TiO₂ well rationalizes the role of nature of metal for conduction developed by formation of Schottky barriers⁵⁹ at different M-TiO₂ interface.

Table 1. Chemical, elemental, electronic and photocatalytic parameters of M-TiO₂ composites.

Catalyst	Band Gap (eV)	Conductance $\times 10^{-7}$ (S)	$e^- - h^+$ recombination time (μ s)	Oxidation state (from XPS analysis)	Photo-oxidation efficiency, k (min^{-1})	
					BZ	NBZ
TiO ₂	3.12	1.65±0.20	18	--	$8.5 \times 10^{-3} \pm 0.13$	$6.2 \times 10^{-3} \pm 0.21$
Au-TiO ₂	2.96	2.5±0.30	24	Au ⁰	$2.7 \times 10^{-2} \pm 0.12$	$2.5 \times 10^{-2} \pm 0.13$
Ag-TiO ₂	2.91	2.7±0.25	27	Ag ⁰	$4.0 \times 10^{-2} \pm 0.11$	$6.1 \times 10^{-2} \pm 0.14$
Cu-TiO ₂	2.90	2.1±0.32	20	Cu ⁺²	$1.93 \times 10^{-2} \pm 0.20$	$1.50 \times 10^{-2} \pm 0.10$

3.7 Time resolved spectroscopy

The dynamics of charge recombination time and interparticle electron transfer between metal and semiconductor is a very important criterion to be considered which can be easily understood through time-resolved spectroscopy. Though reports are available regarding the electron charge carrier time of NC as a function of shape and size of the semiconductors⁶⁰, still the influence of

nature of metal onto the band edge and trapping states still remains a challenge. The charge carrier's relaxation dynamics of M-TiO₂ relative to P25-TiO₂ are shown in Fig. 6b, which is measured by pulse excitation method. Samples were exposed to nitrogen laser (wavelength = 390 nm) and time resolved decay curves are obtained from where lifetime values of the various excited states have been calculated. The average lifetime τ_{av} , is related to band edge lifetime τ_1 and trapping or defect states given by the following equation⁵⁹:

$$\tau_{av} = \frac{a_1 \tau_1 + a_2 \tau_2}{a_1 + a_2}$$

Where a_1 and a_2 represent the amplitude of band edge, and trapping state emission, respectively. The estimated average lifetimes are $\approx 18, 20, 24$ and $27 \mu\text{s}$ for bare P25-TiO₂, Cu-TiO₂, Au-TiO₂ and Ag-TiO₂, respectively. An increase in relaxation time of photoexcited electron-hole pairs is observed with the change in the nature of the metal NPs. It has been reported^{8,61} that Ag metal has a maximum capacity to capture and store electrons and acts as a better electron sink. Although metal nanoparticles act as better electron sink. It is well known that nonradiative recombination was mostly promoted in the presence of metal nanoparticles. However, a decrease in the nonradiative recombination has been observed might be due to the presence of more electrons in the conduction band of metal-TiO₂ nanocomposites. These excess electrons are produced due to the electrons injected in the conduction band of TiO₂ after excitation (with nitrogen laser, wavelength ≈ 390 nm) of the metal nanoparticles at a wavelength close to their surface plasmon band as reported by Grabowska et al³⁰. Other probable reason for this lower intensity non-radiative recombination could be improper electrical junction between metal nanoparticles and TiO₂ surface because of low temperature sintering of M-TiO₂ composite system.

3.8 Photocatalytic activity

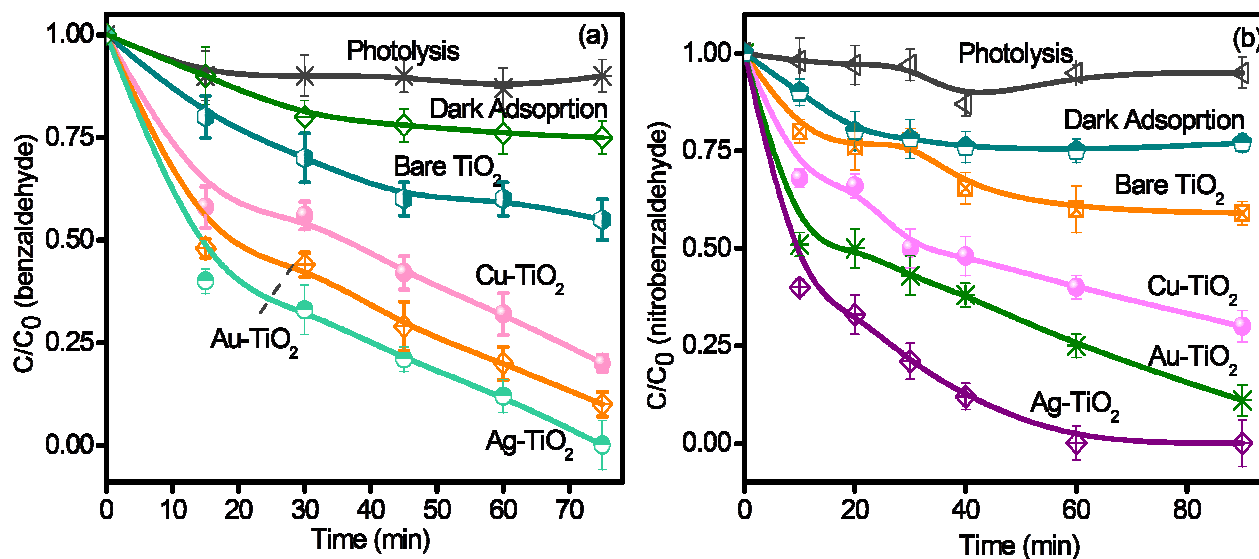


Figure 7. Time course graph for the photocatalytic degradation of (a) benzaldehyde and (b) nitrobenzaldehyde by bare and M-TiO₂ nanocomposites under direct sunlight irradiation.

The comparative photocatalytic activity of M-TiO₂ composites as a function of nature of metal NP (as shown in Scheme 1) has been investigated by oxidizing BZ and NBZ under sunlight irradiation and plots for their extent of degradation (C/C_0) versus time has been displayed in Fig. 7, where C is the absorbance of substrate solution at each time interval of irradiation and C_0 is the absorbance of the initial concentration. The stability of both substrates was primarily tested under sunlight irradiation without the addition of any catalyst which confirms their non-degradable nature. Moreover, substrates showed a negligible loss in the concentration during the dark reaction catalyzed by TiO₂ and M-TiO₂ composites that might be due to adsorption.

The photooxidation process follows pseudo first-order kinetics using a simplified Langmuir–Hinshelwood model, $r = -dC/dt = k(KC)/(1 + KC)$ where r is the initial rate of photocatalytic degradation ($\text{mol l}^{-1}\text{min}^{-1}$), C is the concentration of the reactant (mol l^{-1}), t is the irradiation time (min), k is the rate constant and K is the Langmuir–Hinshelwood adsorption constant. At

low concentration, KC can be neglected with respect to 1 and one gets the simplified equation: $r = -dC/dt = kKC$ or $C/C_0 = e^{-kKt} = e^{-kt}$ where k is the apparent rate constant of the pseudo-first order (min^{-1}) reaction.

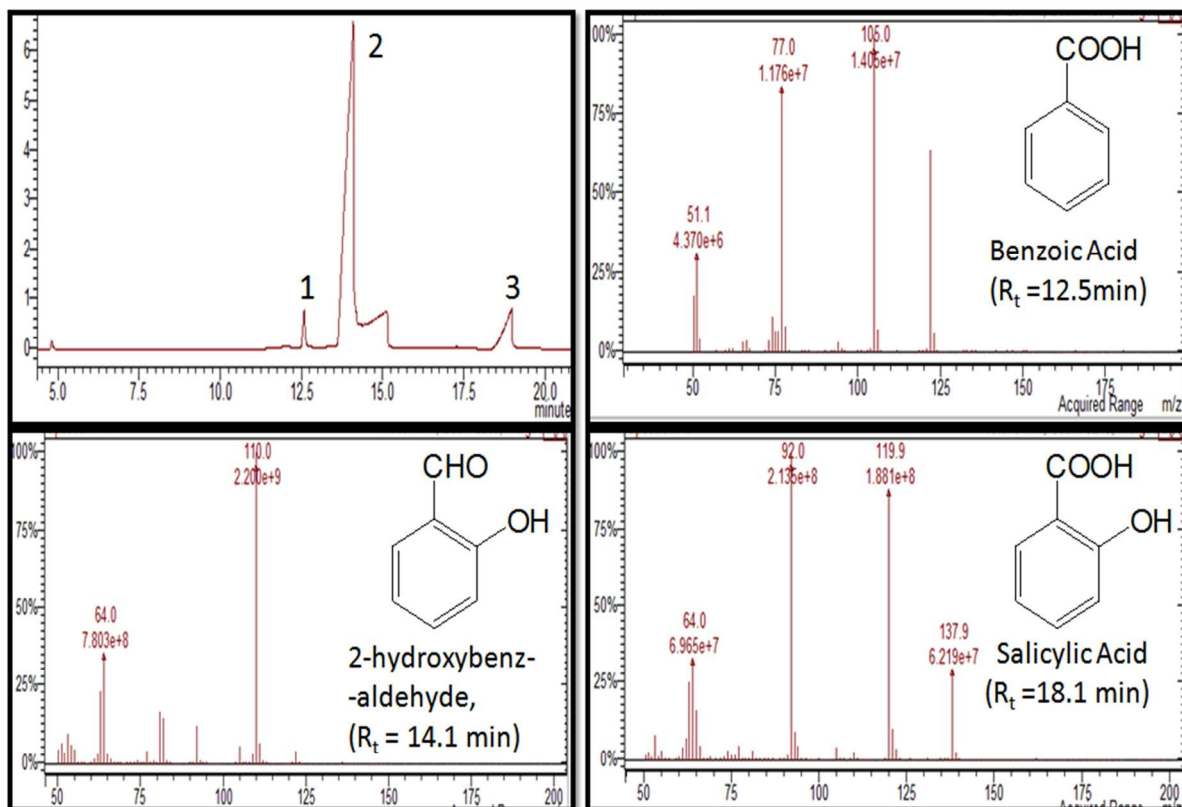
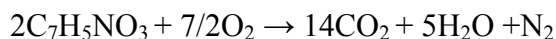
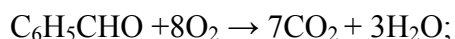


Figure 8. GC chromatograph for oxidation of benzaldehyde using Au-TiO₂ composite after 75 min of irradiation and mass spectra of identified compound; *inset* structural formula and retention times of identified compounds.

The apparent rate constant (k) was calculated (Fig. 7a) and was observed highest for Ag-TiO₂ ($4 \times 10^{-2} \text{ min}^{-1}$) as compared to $2.7 \times 10^{-2} \text{ min}^{-1}$ for Au-TiO₂ and $1.93 \times 10^{-2} \text{ min}^{-1}$ for Cu-TiO₂ during BZ photooxidation. In a similar way, Ag-TiO₂ displayed maximum NBZ photodegradation competence ($\approx 99\%$) relative to the lowest (40%) for P25-TiO₂. The GC-MS (Fig. 8) analysis revealed that mineralization of BZ yield various intermediates such as benzoic acid ($m/z = 122$, $R_t = 12.5 \text{ min}$), 2-hydroxybenzaldehyde ($m/z = 122.12$, $R_t = 14.1 \text{ min}$) and

salicylic acid ($m/z = 138$, $R_t = 18.3$ min). The exact % age for BZ and NBZ mineralization was also perceived through quantitative determination of the CO_2 evolution (Fig. 9a). It has been suggested that if a molecule of BZ ($\text{C}_6\text{H}_5\text{CHO}$) and NBZ ($\text{C}_7\text{H}_5\text{NO}_3$) was completely mineralized, it will give CO_2 and water as per following equation:



Although other species like nitrogen (for NBZ) was not measured, but the measured CO_2 formation confirmed the photodegradation of BZ and NBZ by various M-TiO₂ nanocomposites under visible light irradiation. It was found that Ag-TiO₂ catalyst produced the highest amount of $\text{CO}_2 \approx 38\%$ in 3 h in contrast to 29.8% and 21.5% by Au-TiO₂ and Cu-TiO₂, respectively. A similar trend has been seen for NBZ photodecomposition as displayed in Fig. 9a.

All the above results indicate that M-TiO₂ composites always exhibit higher photocatalytic efficiency than commercial P25-TiO₂ of the same total mass (≈ 20 mg), specifying enhanced photocatalytic activity due to the presence of plasmonic metals as shown in Scheme 1. It has been reported that TiO₂-Au nanospheres relative to commercial TiO₂ (P25) and TiO₂ nanospheres offer 1.8 and 1.2 fold higher activity for the photo degradation⁶² of methylene blue and 4.3 and 1.8 times higher for the reduction of Cr^{6+} . The TiO₂ photoactivity has been found to be drastically enhanced on loading different sizes of Au nanospheres and the effective amount (0.01 wt%) of Au atom required for maximum photocatalytic activity of TiO₂ is 100 times less than the traditional prerequisite of 1–2 wt% metal deposition⁴⁶. Zhou et al.⁶³ prepared Au-TiO₂ nanocomposites for photocatalytic degradation of Rhodamine-B dye in water and observed higher photocatalytic activity than that of pristine TiO₂ nanoparticles due to the surface plasmon resonance.

The enhancement in the M-TiO₂ composites relative to TiO₂ in visible light can be explained as per reported mechanisms^{1-10,21} and displayed in scheme 1. The noble metal NPs act as sensitizers, absorb visible light due to their SPR band, resulted in the formation of the electrons and holes on the metal NPs surface which assist in the oxidation of reactant substrates. The electrons are transferred to the adsorbed oxygen molecules via. conduction band of TiO₂ resulting in the formation of superoxide radicals. These radicals upon assistance with CB electrons combine to produce H₂O₂ that ultimately producing hydroxyl radicals. Both hydroxyl and superoxide radicals are strong oxidants, and therefore oxidize BZ and NBZ, resulting in the formation of intermediate organic species and subsequently mineralize to water and CO₂. Therefore, lowest photocatalytic efficiency of bare TiO₂ (anatase:rutile ≈ 70:30) relative to M-TiO₂ nanocomposites can be accounted to its insufficiency of absorbing visible light.

The above results also indicate that whether the morphological aspects of NPs are similar, still variation in the enhancement of TiO₂ photoactivity has been observed, which can be attributed to the metallic nature of NPs. Therefore, the nature of metal NP, their dissimilar charge carrier potency, reduction potential, Fermi level position, oxidation state, etc. contributed towards dissimilar photoactivity of hybrid NC. In this study, the comparison among plasmonic (Au, Ag and Cu) nanomaterials have displayed that Ag-TiO₂ NC offers superior photoefficiency over Au and Cu-TiO₂ composites. The highest conductance in Ag-TiO₂ NC (Fig. 6a, 2.7×10^{-7} μS), the least work function of Ag metal (ESI-table 1) and relative near Fermi level position to CB of TiO₂ favors quick transference of electrons from Ag to TiO₂ than other composite systems. The AgNS loading also prolonging the lifetime of charge carriers and, thereby, increased the relaxation time of charge species of TiO₂ (Fig. 6b). The maximum recombination time for photoproduced charge carriers in Ag-TiO₂ brings more formation of highly oxidative

superoxide and hydroxyl radicals and hence, highest photooxidation ability. Undoubtedly, the observed (Ag > Au > Cu) photocatalytic behavior of metal-NPs is opposite to that expected from their reduction potentials. This surprising trend can be explained from XPS data that reveals +2 oxidation state for Cu in Cu-TiO₂ composite, while zero for Ag and Au, due to which Cu first acquires photoproduced electrons from TiO₂ making availability of holes for production of only OH radicals. Whereas, for Ag and Au-TiO₂ (zero oxidation state) composites, there is formation of two highly oxidative species viz., hydroxyl and superoxide radicals that bring higher photoactivity for these composites.

The reusability and stability of the prepared M-TiO₂ composites were also examined by photodegradation of NBZ for five cycles to ensure any loss in the activity (Fig. 9b). The photocatalytic activity of Au-TiO₂, Ag-TiO₂ and Cu-TiO₂ of the last cycle maintained ≈80%,

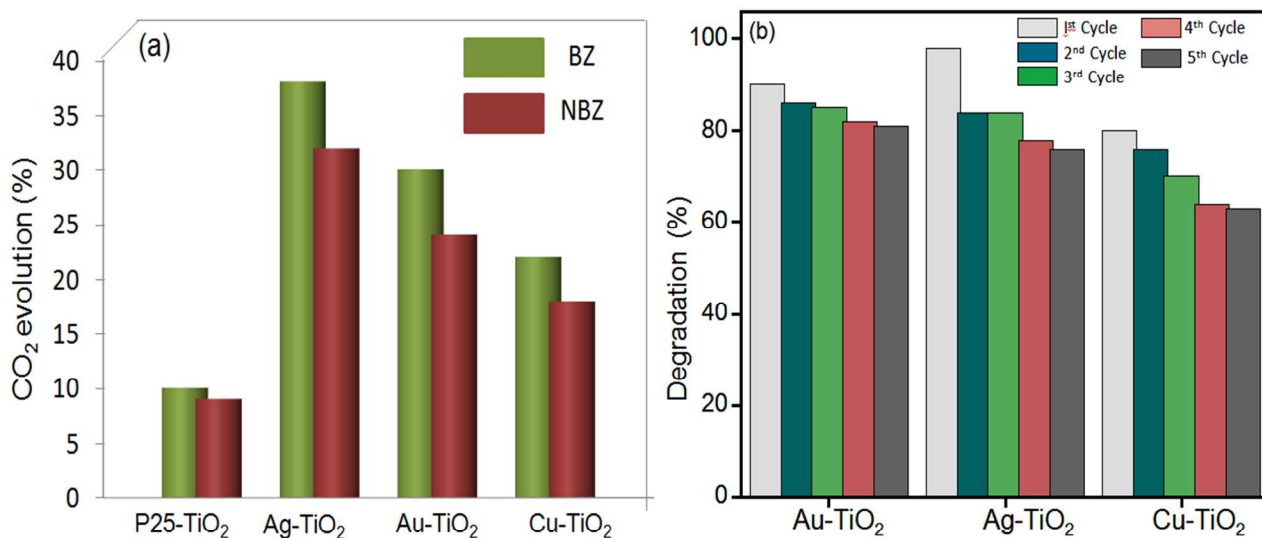


Figure 9. Percentage of CO₂ evolution on photodegradation of benzaldehyde (BZ) and nitrobenzaldehyde (NBZ) by using various M-TiO₂ nanocomposites after 3 h of sunlight irradiation and (b) nitrobenzaldehyde degradation (%) after recycling with M-TiO₂ composites under visible light irradiation.

75%, and 60% of the original photocatalytic activity, respectively. TEM image (ESI-Fig.S6) of

Au-TiO₂ NC after recycling showed the presence of metal nanoparticles (dark colored particles) on TiO₂ matrix (gray colored particles) which confirms the interaction between them.

4. Conclusion

This study provides a detailed account on the interfacial properties of coinage metal nanoparticles impregnated TiO₂ composites for improved co-catalysis, and promoting its light sensitivity to visible/sun light irradiation as compared to conventional metal deposited titania interface. The plasmonic interaction of as-prepared coinage metal nanospheres co-catalysts of similar size (3-5 nm) imparted to TiO₂ for the photooxidation are found govern the interfacial energetics and charge transfer kinetics depending on the nature of plasmonic metal, and its work function or Fermi energy etc. The Ag-TiO₂ heterojunction has been found to exhibit enhanced photocatalytic activity relative to Au and Cu-TiO₂ that are explained by the current-voltage characteristics, and charge recombination time etc. Thus, it is evident that quantum size particles of coinage metal could utilize solar energy to a higher extent for efficient photooxidation reactions.

Acknowledgments:

R. Kaur gratefully thanks to the Department of Science and Technology, Government of India, for financial support under Women Young Scientist Fellowship Scheme (No.SR/WOS-A/CS-61/2012).

References

- [1] S.T. Kochuveedu, Y.H. Jang and D.H. Kim, Chem. Soc. Rev., 2013, 42, 8467-8493.
- [2] P. Wang, B. Huang, Y. Daia and M.H. Whangbo, Phys. Chem. Chem. Phys., 2012, 14, 9813-9825.
- [3] M.M. Khan, S.A. Ansari, J. Lee and M.H. Cho, J. Ind. Eng. Chem., 2013, 19, 1845-1850.

- [4] S. Sarina, E.R. Waclawik and H. Zhu, *Green Chem.*, 2013, 15, 1814-1833.
- [5] S.F. Chen, J.P. Li, K. Qian, W.P. Xu, Y. Lu, W.X. Huang and S.H. Yu, *Nano Res.*, 2010, 3, 244-255.
- [6] S. Linic, P. Christopher and D.B. Ingram, *Nat. Mater.*, 2011, 10, 911-921.
- [7] J.C. Scaiano and K. Stampelcoskie, *J. Phys. Chem. Lett.*, 2013, 4, 1177-1187.
- [8] W.T. Chen, Y.J. Hsu and P.V. Kamat, *J. Phys. Chem. Lett.*, 2012, 3, 2493-2499.
- [9] Z. Zheng, B. Huang, X. Qin, X. Zhang, Y. Dai and M.H. Whangbo, *J. Mater. Chem.*, 2011, 21, 9079-9087.
- [10] X. Zhou, G. Liu, J. Yu and W. Fan, *J. Mater. Chem.*, 2012, 22, 21337-21354.
- [11] A. Pearson, S. Bhosale, S.K. Bhargava and V. Bansal, *Appl. Mater. Inter.*, 2013, 5, 7007-7013.
- [12] Y. Ishii, Y. Kanamori, T. Kawashita, I. Mukhopadhyay and S. Kawasaki, *J. Phys. Chem. Solids*, 2010, 71, 511-513.
- [13] H. Zhu, X. Ke, X. Yang, S. Sarina and H. Liu, *Angew. Chem. Int. Ed.*, 2010, 49, 9657-9661.
- [14] H. Zhu, X. Chen, Z. Zheng, X. Ke, E. Jaatinen, J. Zhao, C. Guo, T. Xie and D. Wang, *Chem. Commun.*, 2009, 7524-7526.
- [15] X. Chen, Z. Zheng, X. Ke, E. Jaatinen, T. Xie, D. Wang, C. Guo, J. Zhao and H. Zhu, *Green Chem.*, 2010, 12, 414-419.
- [16] H. Li, Z. Bian, J. Zhu, Y. Huo, H. Li and Y. Lu, *J. Am. Chem. Soc.*, 2007, 129, 4538-4539.
- [17] X.H. Yang, H.T. Fu, K. Wong, X.C. Jiang and A.B. Yu, *Nanotechnology*, 2013, 24, 415601.
- [18] K.Y. Song, Y.T. Kwon, G.J. Choi and W.I. Lee, *Bull. Korean Chem. Soc.*, 1999, 20, 957-960.

- [19] L. Liu, S. Ouyang and J. Ye, *Angew. Chem.*, 2013, 125, 6821-6825.
- [20] N. Zhou, L. Polavarapu, N. Gao, Y. Pan, P. Yuan, Q. Wang and Q.H. Xu, *Nanoscale*, 2013, 5, 4236-4241.
- [21] R. Sellappan, M.G. Nielsen, F.G. Posada, P.C.K. Vesborg, I. Chorkendorff and D. Chakarov, *J. Catal.*, 2013, 307, 214-221.
- [22] Y. Tian and T. Tatsuma, *J. Am. Chem. Soc.*, 2005, 127, 7632-7637.
- [23] A.Z. Jurek, E. Kowalska, J.W. Sobczak, W. Lisowski, B. Ohtani and A. Zaleskaa, *Appl. Catal. B: Environ.*, 2011, 101, 504-514.
- [24] Y. Tian and T. Tatsuma, *Chem. Commun.*, 2004, 1810-1811.
- [25] Z.W. Seh, S. Liu, M. Low, S. Zhang, Z. Liu, A. Mlayah and M. Han, *Adv. Mater.*, 2012, 24, 2310-2314.
- [26] O.T. Alaoui, A. Herissana, C.L. Quoca, M.M. Zekria, S. Sorguesa, H. Remita, C.C. Justina, *J. Photochem. Photobiol. A.*, 2012, 242, 34-43.
- [27] J. Yu, G. Dai and B. Huang, *J. Phys. Chem. C*, 2009, 113, 16394-16401.
- [28] E. Kowalska, K. Yoshiiri, Z. Wei, S. Zheng, E. Kastl, H. Remita, B. Ohtani, S. Rau, *Appl. Catal. B.*, 2014, in press, doi:10.1016/j.apcatb.2014.10.003.
- [29] E. Kowalska, Z. Wei, B. Karabiyik, A. Herissan, M. Janczarek, M. Endo, A. Markowska-Szczupak, H. Remita, B. Ohtani, *Catal. Today*, in press, <http://dx.doi.org/10.1016/j.cattod.2014.10.038>.
- [30] E. Grabowska, A. Zaleska, S. Sorgues, M. Kunst, A. Etcheberry, C. Colbeau-Justin, H. Remita, *J. Phys. Chem. C*, 2013, 117, 1955-1962.
- [31] Z. Hai, N.E. Kolli, D.B. Uribe, P. Beaunier, M.J. Yacaman, J. Vigneron, A. Etcheberry, S. Sorgues, C. Colbeau-Justin, J. Chen, H. Remita, *J. Mater. Chem. A*, 2013, 1, 10829-10835.

- [32] S. Ghosh, N.A. Kouame, L. Ramos, S. Remita, A. Dazzi, A.D. Besseau, P. Beaunier, F. Goubard, P.H. Aubert and H. Remita, *Nat. Mater.*, 2015, 14, 505-511.
- [33] D. Tsukamoto, Y. Shiraishi, Y. Sugano, S. Ichikawa, S. Tanaka and T. Hirai, *J. Am. Chem. Soc.*, 2012, 134, 6309-6315.
- [34] H. Choi, W.T. Chen and P.V. Kamat, *ACS Nano*, 2012, 6, 4418-4427.
- [35] M. Rycenga, C.M. Cobley, J. Zeng, W. Li, C.H. Moran, Q. Zhang, D. Qin and Y. Xia, *Chem. Rev.*, 2011, 111, 3669-3712.
- [36] C. Li, D. Li, G. Wan, J. Xu and W. Hou, *Nanoscale Res. Lett.*, 2011, 6, 1-10.
- [37] Ratyakshi and R.P. Chauhan, *Asian J. Chem.*, 2009, 21, 113-116.
- [38] J. Kimling, M. Maier, B. Okenve, V. Kotaidis, H. Ballot and A. Plech, *J. Phys. Chem. B*, 2006, 110, 15700-15707.
- [39] M. Samim, N.K. Kaushik and A. Maitra, *Bull. Mater. Sci.*, 2007, 30, 535-540.
- [40] K. Cheirmadurai, S. Biswas, R. Murali, P. Thanikaivelan, *RSC Adv.*, 2014, 4, 19507-19511.
- [41] N. Gupta and B. Pal, *J. Mol. Catal. A: Chem.*, 2013, 371, 48-55.
- [42] I. Tunc, M. Bruns, H. Gliemann, M. Grunze and P. Koelsch, *Surf. Interface Anal.*, 2010, 42, 835-841.
- [43] T. Hirakawa and P.V. Kamat, *Langmuir*, 2004, 20, 5645-5647.
- [44] M. Sahu and P. Biswas, *Nanoscale Res Lett.*, 2011, 6, 1-14.
- [45] B. Choudhury, M. Dey and A. Choudhury, *Int. Nano Lett.*, 2013, 3, 1-8.
- [46] R. Kaur, B. Pal, *J. Mol. Catal. A: Chem.*, 2012, 355, 39-43.

- [47] A. Lewera, L. Timperman, A. Roguska, N.A. Vante, *J. Phys. Chem. C*, 2011, 115, 20153–20159.
- [48] D.W. Goodman, *Catalysis Letters*, 2005, 99, 1–2.
- [49] M.A. Uppal, A. Kafizas, M.B. Ewing, I.P. Parkin, *J. Mater. Chem. A*, 2013, 1, 7351-7359.
- [50] Mohd. A.M. Khan, S. Kumar, M. Ahamed, S.A. Alrokayan, M.S. AlSalhi, *Nanoscale Res Lett.*, 2011, 6, 434-442.
- [51] I.S. Grover, S. Singh and B. Pal, *Appl. Surf. Sci.*, 2013, 280, 366-372.
- [52] N. Kruse and S. Chenakin, *Appl. Catal. A: Gen.*, 2011, 391, 367-376.
- [53] B. Cheng, Y. Le and J. Yu, *J. Hazard. Mater.*, 2010, 177, 971-977.
- [54] M.H. Ahmed, T.E. Keyes, J.A. Byrne, *J. Photoch. Photobio. A*, 254 (2013) 1-11.
- [55] S.S. Mandal and A.J. Bhattacharyya, *J. Chem. Sci.*, 2012, 124, 969-978.
- [56] M. Ganguly, A. Pal and T. Pal, *J. Phys. Chem. C*, 2011, 115, 22138-22147.
- [57] T. Bala, A. Singh, A. Sanyal, C.O. Sullivan, F. Laffir, C. Coughlan and K.M. Ryan, *Nano Res.*, 2013, 6, 121-130.
- [58] C.Y. Tsai, H.C. Hsi, T.H. Kuo, Y.M. Chang and J.H. Liou, *Aerosol Air Qual. Res.*, 2013, 13, 639-648.
- [59] G.S. Lotey and N.K. Verma, *J. Nanopart. Res.*, 2011, 13, 5397-5405.
- [60] I.S. Grover, S. Singh and B. Pal, *J. Nanosci. Nanotechnol.*, 2015, 15, 1490-1498.
- [61] J. Qi, X. Dang, P.T. Hammond, A.M. Belcher, *ACS Nano*, 2011, 5, 7108–7116.
- [62] R. Ravindranath, P. Roy, A.P. Periasamy, H.T. Chang, *RSC Adv.*, 2014, 4, 57290-57296.
- [63] M. Zhou, J. Zhang, B. Cheng, H. Yu, *Int. J. Photoenergy*, 2012, 532843, 1-10.

Graphical Abstract:

